A Synthetic, Structural, Spectroscopic and Computational Study of Alkali Metal–Thioether, -Selenoether and -Telluroether Interactions

Novan A. G. Gray, Ignacio Vargas-Baca and David J. H. Emslie*

Department of Chemistry and Chemical Biology, McMaster University, Hamilton, Ontario L8S 4M1, Canada

Supporting Information Placeholder

ABSTRACT: The rigid thioether- and selenoether-containing ligands, 4,5-bis(phenylsulfido)-2,7,9,9-tetramethylacridan (H[AS_2^{Ph2}] (**1**)) and 4,5-bis(phenylselenido)-2,7,9,9-tetramethylacridan (H[ASe_2^{Ph2}] (**2**)) were deprotonated with one equiv. of ^{n}BuLi to afford dimeric lithium complexes [Li(AE_2^{Ph2})]$_2$ (E = S (**3**), Se (**4**)), or with one equiv. of KCH_2Ph to afford the previously reported potassium complexes [K(AS_2^{Ph2})(dme)]$_x$ (**5**) and [K(ASe_2^{Ph2})(dme)$_2$] (**6**). Attempts to prepare a direct telluroether analogue of **1**-**2** were unsuccessful. However, the bulky selenoether- and telluroether-containing pro-ligands 4,5-bis(2,4,6-triisopropylphenylselenido)-2,7,9,9-tetramethylacridan (H[ASe_2^{Tripp2}] (**7**)) and 4,5-bis(2,4,6-triisopropylphenyltellurido)-2,7,9,9-tetramethylacridan (H[ATe_2^{Tripp2}] (**8**)) were accessed via the reaction of 4,5-dibromo-2,7,9,9-tetramethylacridan with three equiv. of ^{n}BuLi, followed by the addition of two equiv. of the corresponding diaryl dichalcogenide and quenching with dilute $HCl_{(aq)}$. The new selenoether- and telluroether-containing pro-ligands were subsequently deprotonated using KCH_2Ph to afford [K(AE_2^{Tripp2})(dme)$_2$] (E = Se (**9**), Te (**10**)). Compounds **1**-**10** were characterized by ^{1}H, ^{13}C{^{1}H}, ^{77}Se{^{1}H}, ^{125}Te{^{1}H} and ^{7}Li NMR spectroscopy, where applicable, and single crystal X-ray structures were obtained for all lithium and potassium complexes (**3**-**6** and **9**-**10**). DFT calculations were also performed to assess the nature of bonding between the hard group 1 cations and the soft chalcogenoethers.

INTRODUCTION

Ether donors are ubiquitous in the coordination chemistry of the alkali metals, with nearly 40 % of all crystallographically-characterized group 1 complexes containing M–OR_2 (M = Li-Cs) linkages.[†] The favourability of these interactions arises from the hard-hard pairing between electropositive group 1 cations and electronegative oxygen donors; interactions which are primarily ionic in nature, in accordance with hard soft acid base (HSAB) principles.[1] By contrast, alkali metal compounds featuring heavier chalcogenoether donors are scarce, with almost all examples confined to thioethers.

The only structurally characterized group 1 compounds bearing monodentate thioether ligands are a series of lithium cuprate compounds which incorporate both terminal and bridging SMe_2 ligands,[2-4] and [Li_2(*m*-H_2BAr_2)$_2$(SMe_2)$_4$].[5] Neutral oxa-thia macrocycles such as 1,4,10,13-tetraoxa-7,16-dithiacyclooctadecane ([18]aneO_4S_2) and/or 1,10-dioxa-4,7,13,16-tetrathiacyclooctadecane ([18]aneO_2S_4) have been used to access a series of Li, Na, K, Rb and Cs complexes featuring M–SR_2 linkages.[6-12] Additionally, [Na([24]aneS_8)][B{$C_6H_3(CF_3)_2$-3,5}$_4$] ([24]aneS_8 = 1,4,7,10,13,16,19,22-octathiacyclotetracosane), which features an octadentate thiacrown, is unique as the only s-block complex in which the metal is coordinated exclusively to thioether donors.[13] Other alkali metal thioether complexes feature more complex multidentate ligands, including thiacalixarenes,[14-19] and acyclic ligands containing a mixture of anionic (e.g. R_3C^-, R_2N^-, RO^-) donors and thioether groups.[20-23]

In contrast to group 1 thioether complexes, selenoether complexes are limited to just two examples; [M([18]aneO_4Se_2)][B{$C_6H_3(CF_3)_2$-3,5}$_4$] (M = Na and K),[6] featuring the 1,4,10,13-tetraoxa-7,16-diselenacyclooctadecane macrocycle. In the solid-state, the ligands in both compounds are κ^6-coordinated, providing the only reported examples of alkali metal–selenoether interactions. Notably, Li, Rb and Cs [18]aneO_4Se_2 complexes were not reported, despite the accessibility of the thioether-containing [18]aneO_4S_2 analogues.

Group 2 selenoether complexes are also limited to just a handful of examples. Reid et al. reported neutral [MI_2([18]aneO_4Se_2)] (M = Ca or Sr),[24] and dicationic [M([18]aneO_4Se_2)($MeCN)_2$][BAr^F]$_2$ (M = Mg, Ca, Sr) and [Ba([18]aneO_4Se_2)(acacH)(MeCN)][BAr^F]$_2$.[25] X-ray crystal structures of the neutral calcium complex and the dicationic calcium, strontium and barium species (structures of the neutral strontium and dicationic magnesium compounds were not reported) feature κ^6-coordination of the [18]aneO_4Se_2 ligand, analogous to the aforementioned Na and K complexes. Additionally, adventitious hydrolysis during attempted crystallization of [SrI_2([18]aneO_4Se_2)] and [Mg([18]aneO_4Se_2)($MeCN)_2$][BAr^F]$_2$ afforded crystals of [Sr($H_2O)_3$([18]aneO_4Se_2)]I_2 and [Mg(κ^3-[18]aneO_4Se_2)($H_2O)_2$(MeCN)][BAr^F]$_2$, respectively. Interestingly, in the solid-state structure of [Sr($H_2O)_3$([18]aneO_4Se_2)]I_2, the iodide ligands have been displaced by three water molecules, but the metal retains hexadentate coordination to the neutral [18]aneO_4Se_2 macrocycle. By contrast, in [Mg(κ^3-[18]aneO_4Se_2)($H_2O)_2$(MeCN)][BAr^F]$_2$, replacement of one acetonitrile ligand by two water molecules resulted in a κ^3-*O,O,Se*-coordination mode of the [18]aneO_4Se_2 macrocycle.

Group 1 or 2 complexes employing acyclic selenoether-containing ligands have not been reported. Additionally, there are no reports of s-block telluroether complexes, and it is notable that attempted reactions of a telluroether analogue of the [18]aneO_4Se_2 macrocycle, [18]aneO_4Te_2, with CaI_2 or SrI_2 in MeCN resulted in no observable reaction.[24]

Our group has previously employed rigid pincer ligands to prepare a range of organometallic and coordination complexes of electropositive actinide[26-33] and rare earth[34-40] elements. In addition, we recently reported the rigid thioether- and selenoether-

containing ligands 4,5-bis(phenylsulfido)-2,7,9,9-tetramethylacridan (H[AS_2^{Ph2}] (**1**)) and 4,5-bis(phenylselenido)-2,7,9,9-tetramethylacridan (H[ASe_2^{Ph2}] (**2**)), their deprotonation to generate the potassium salts, and subsequent reactivity with [UI_4(1,4-dioxane)$_2$] to afford [(AS_2^{Ph2})$_2UI_2$] and [(ASe_2^{Ph2})$_2UI_2$]. These uranium(IV) complexes feature rare examples of uranium–thioether bonds and the first examples of structurally authenticated uranium–selenoether bonds, respectively.[41]

The AE_2^{Ph2} (E = S or Se) ligands harness the rigidity of the tricyclic acridanide ligand backbone and the positioning of the flanking chalcogenoether donors (with direct attachment of the donor atoms to the anionic ligand backbone) to encourage κ^3-*SNS*- or κ^3-*SeNSe*-coordination to electropositive metal centres. Herein, we report the synthesis, solution characterization, and solid-state structures of lithium and potassium complexes of the AS_2^{Ph2} and ASe_2^{Ph2} ligands, as well as bulky 2,4,6-triisopropylphenyl-substituted selenoether- and telluroether-containing analogues of H[AS_2^{Ph2}] and H[ASe_2^{Ph2}], and their potassium salts. DFT calculations to probe the nature of alkali metal–ER_2 (E = S, Se and Te) bonding in these complexes are also described.

RESULTS AND DISCUSSION

Synthesis and solid-state structures

Deprotonation of the H[AS_2^{Ph2}] (**1**) and H[ASe_2^{Ph2}] (**2**) pro-ligands with one equivalent of ^{n}BuLi at –78 °C afforded the lithium complexes [Li(AS_2^{Ph2})]$_2$ (**3**) and [Li(ASe_2^{Ph2})]$_2$ (**4**) as pale yellow-orange powders in 98 and 89 % yield, respectively (Scheme 1). X-ray quality crystals of **3**·2 toluene and **4** were obtained from toluene solutions layered with hexanes at –30 °C. Additionally, [K(AS_2^{Ph2})(dme)]$_x$ (**5**) and [K(ASe_2^{Ph2})(dme)$_2$] (**6**) were prepared by deprotonation of **1** and **2** using KCH_2Ph, as previously reported, and X-ray quality crystals were obtained from dme solutions layered with hexanes at –30 °C.

Scheme 1. Synthesis of lithium complexes **3** and **4**.

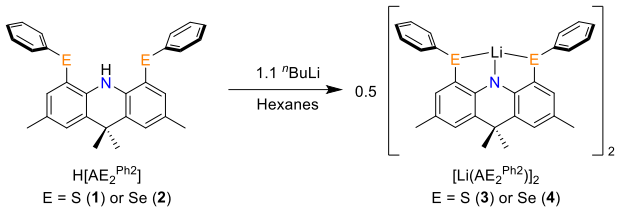

In the solid-state, lithium complexes **3** and **4** are isostructural dimers with rhombus-shaped Li_2N_2 cores (Figure 1). Each lithium cation is located in the plane of one of the ligands, and above the plane of the other ligand, resulting in C(7)–N(1)–Li(1) and C(7)–N(1)–Li(1') angles of 171 and 102° in **3**, and C(16)–N(1)–Li(1) and C(16)–N(1)–Li(1') angles of 174 and 96° in **4**, respectively. The geometry about the lithium cations can best be described as distorted disphenoidal, according to SHAPE analysis, with the sulfur or selenium donors in axial sites.

For compound **3**, the Li–N distance within the plane of each ligand is 1.983(4) Å, while the Li–N bonds linking the two monomeric units are slightly longer, at 2.119(4) Å.§ The AS_2^{Ph2} ligand backbone is bent away from the Li_2N_2 core of the dimer, with a ligand backbone bend angle of 39° (defined as the angle between the planes of the two acridanide aryl rings). The Li–S distances of 2.494(4) and 2.497(4) Å in **3**‡ are comparable to the Li–S distances found in Power's complexes [$Li_2Cu_2Ph_4(SMe_2)_3$], [$Li_3(CuPh_2)(CuPh_3)(SMe_2)_4$], [$Li_5(CuPh_2)_3(CuPh_3)(SMe_2)_4$] and [$Li_4Ph_4(SMe_2)_4$] (2.445(9)-2.635(4) Å)[3], and to those found in the four-coordinate amido-bridged lithium centres in the 2-(phenylthiol)phenyl(tren) (tren = tris{2-aminoethyl}amine) thioether complex [Li_3{$N(CH_2CH_2N(C_6H_4SPh\text{-}2)_3$}$(THF)_2$] (2.510(6) and 2.542(6) Å).[21] The geometry about the sulfur atoms in **3** is pyramidal, with the sum of the C–S–C and C–S–Li angles equal to 295° and 299°.

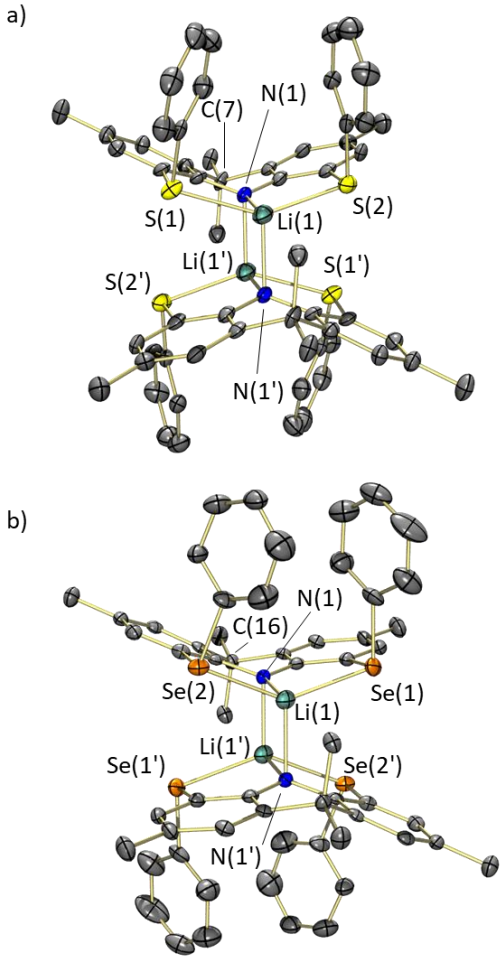

Figure 1. X-ray crystal structures of a) [Li(AS_2^{Ph2})]$_2$·2 toluene (**3**·2 toluene), and b) [Li(ASe_2^{Ph2})]$_2$ (**4**). Lattice solvent and hydrogen atoms are omitted for clarity, and ellipsoids are drawn at 50 % probability.

In selenoether compound **4**, the Li–N distance within the plane of each ligand is 1.987(8) Å while the Li–N distance between monomeric units is 2.111(9) Å.§ These distances are statistically equivalent to those in **3**. The Li–Se bond distances are 2.571(8) and 2.588(8) Å.‡ Other structurally characterized lithium–selenoether interactions are not available for comparison. However, it is interesting to note that the difference between the shortest Li–S distance and the longest Li–Se distance in **3** and **4** is ~0.10 Å, which is less than the difference between the covalent radii of S and Se (0.15 Å).[42] The ligand backbone in **4** is bent by 29°, which is less than in **3**, and the selenium atoms in **4** are more pyramidalized than the sulfur atoms in **3**, with the sum of the C–Se–C and C–Se–Li angles equal to 285° and 291°.

In contrast to the structures of **3** and **4**, the potassium salt of the AS_2^{Ph2} ligand, [K(AS_2^{Ph2})(dme)]$_x$ (**5**), is a 1-dimensional polymer in the solid-state, with potassium cations bridging between AS_2^{Ph2} ligands (Figure 2). The potassium cations are seven-coordinate due to κ^3-*SNS*-coordination to each AS_2^{Ph2} ligand and κ^1-coordination to dme (K–O = 2.749(2) Å)§, and the geometry is

best described as distorted capped trigonal prismatic, with N(1) as the capping atom.

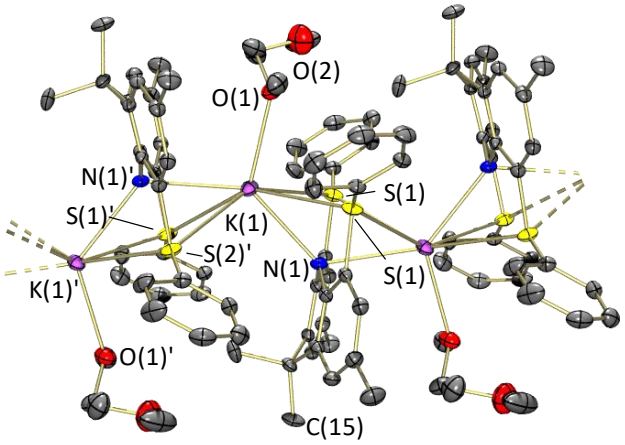

Figure 2. X-ray crystal structure of $[K(AS_2^{Ph2})(dme)]_x$ (**5**) showing a three-monomer segment of the 1-D polymeric structure. The dominant component of a two-part dme disorder is shown. Hydrogen atoms are omitted for clarity, and ellipsoids are drawn at 50 % probability.

The ligand backbone in **5** is bent 31° from planarity, and the potassium atoms are positioned 2.51 Å and 2.58 Å above/below the SNS plane. The N(1)–K(1) distance of 2.816(2) Å is slightly shorter than the N(1)–K(1') distance of 2.942(2) Å,§ and the four K–S distances fall within a fairly narrow range, from 3.2782(8) to 3.3529(8) Å.‡ These distances fall within the span of the K–(μ_2-SR_2) distances (2.832(2)-3.483(4) Å) observed in the potassium–thiacalix[4]arene complex $[K_4(L{\cdot}2H)_2(MeOH)_2(H_2O)_{1.5}]_x$ (L = *p*-*H*-thiacalix[4]arene, "2H" denotes the number of phenolic hydrogens on the ligand).[19]

In contrast to compounds **3**-**5**, $[K(ASe_2^{Ph2})(dme)_2]$ (**6**) is a monomer in the solid-state, featuring a seven-coordinate potassium cation which is κ^3-coordinated to the ASe_2^{Ph2} ligand and κ^2-coordinated to two dme solvent molecules (Figure 3). Potassium sits 2.49 Å below the plane of the SeNSe donors, and the ASe_2^{Ph2} ligand backbone is bent by 29°. The geometry at potassium is best described as distorted capped octahedral. The K–Se distances are 3.352(2) and 3.380(1) Å,‡ which are slightly longer than those in $[K([18]aneO_4Se_2)][BAr^F]$ (3.307(1)-3.3123(7) Å).[6] The K–N distance in **6** is 2.822(5) Å and the K–O distances range from 2.654(4) to 2.813(4) Å.§ The sum of the C–Se–C and C–Se–K bond angles is equal to 313° and 322°, illustrating a lesser degree of pyramidalization of the selenium atoms in **6** compared to lithium complex **4**.

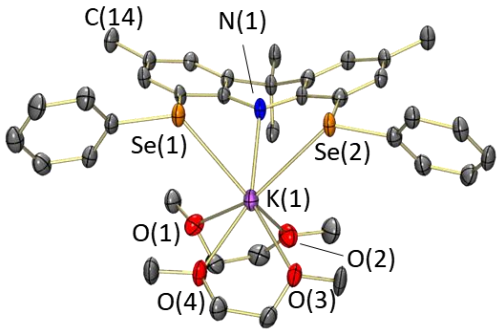

Figure 3. X-ray crystal structure of $[K(ASe_2^{Ph2})(dme)_2]$ (**6**). Hydrogen atoms are omitted for clarity, and ellipsoids are drawn at 50 % probability.

Attempts to synthesize a telluroether analogue of pro-ligand **2**, via trilithiation of 4,5-dibromo-2,7,9,9-tetramethylacridan followed by reaction with two equivalents of Te_2Ph_2, were unsuccessful, perhaps due to the instability of the initially formed lithiated ligand. However, selenium and tellurium analogues of **2** with bulky 2,4,6-triisopropylphenyl (Tripp) substituents on the chalcogen atom, $H[ASe_2^{Tripp2}]$ (**7**) and $H[ATe_2^{Tripp2}]$ (**8**), could be accessed by trilithiation of 4,5-dibromo-2,7,9,9-tetramethylacridan followed by the addition of two equivalents of the appropriate diaryl dichalcogenide and quenching with dilute $HCl_{(aq)}$ (Scheme 2). Compounds **7** and **8** were isolated in 15-21 % yield. The low yields are attributed to workup steps which involve separation of the target compounds from acridan-containing impurities by sublimation at 160 and 170 °C; a process which leaves some of the product trapped in the unsublimed residue. Subsequent deprotonation of **7** and **8** using a slight excess of KCH_2Ph in dme generated the potassium complexes $[K(ASe_2^{Tripp2})(dme)_2]$ (**9**) and $[K(ATe_2^{Tripp2})(dme)_2]$ (**10**) as orange-yellow solids in 88 % (Se) and 98 % (Te) yield, respectively (Scheme 2).

Scheme 2. Syntheses of pro-ligands **7** and **8**, and potassium compounds **9** and **10**.

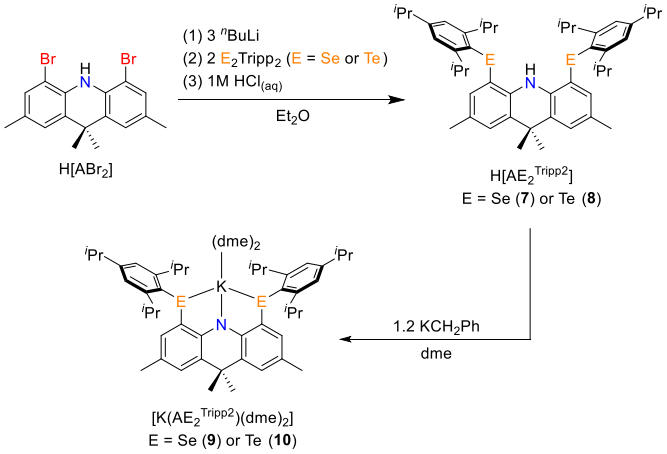

X-ray quality crystals of **9**·0.5 hexanes and **10** were grown from dme solutions layered with hexanes at –30 °C; **9**·0.5 hexanes contains two inequivalent molecules of **9** in the unit cell. The solid-state structures of **9** (Figure 4) and **10** (Figure 5) are qualitatively similar to $[K(ASe_2^{Ph2})(dme)_2]$ (**6**). However, the acridanide backbone of the pincer ligands in **9** and **10** is more planar (*vide infra*), and the dme ligands are positioned so as to minimize unfavourable steric interactions with the flanking 2,4,6-triisopropylphenyl groups.

In compound **9**, one of the two independent molecules in the unit cell features fairly similar K–Se distances of 3.419(2) Å and 3.484(2) Å, whereas the K–Se distances in the other molecule are more dissimilar (3.339(2) Å and 3.633(2) Å).‡ The average K–Se distance of 3.469 Å is ~0.10 Å longer than that in **6** (3.366 Å), presumably due to the greater steric bulk imposed by the Tripp groups in the ASe_2^{Tripp2} ligand. The K–N distances are 2.801(4) Å and 2.840(3) Å, the longer of which belongs to the molecule with the more similar pair of K–Se distances, and the K–O distances range from 2.701(3) to 3.13(1) Å.§ The geometries of the potassium cations in each molecule in the unit cell of **9** are slightly different; the more symmetrical molecule is best described as a distorted pentagonal bipyramid, while the less symmetrical molecule is closer to a distorted capped octahedron, based on SHAPE analysis.

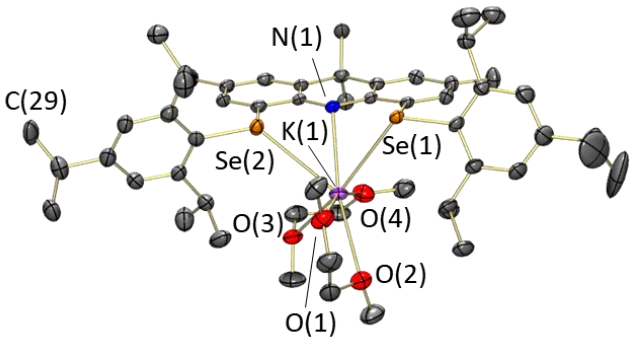

Figure 4. X-ray crystal structure of $[K(ASe_2^{Tripp2})(dme)_2]\cdot 0.5$ hexane (**9**·0.5 hexane). Only one of two inequivalent molecules in the asymmetric unit is shown. Lattice solvent and hydrogen atoms are omitted for clarity, and ellipsoids are drawn at 50 % probability.

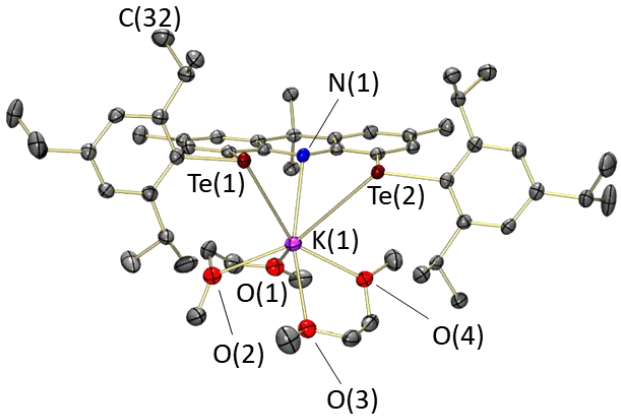

Figure 5. X-ray crystal structure of $[K(ATe_2^{Tripp2})(dme)_2]$ (**10**). Hydrogen atoms have been omitted for clarity, and ellipsoids are drawn at 50 % probability. Bonds are drawn between potassium and tellurium on the basis of K–Te distances that are well within the sum of the Van der Waals radii.‡

The ligand backbone of the more symmetrical molecule is virtually planar with a bend of just 2°, and potassium sits 2.56 Å outside of the ligand binding pocket (the SeNSe plane), while the ligand backbone in the less-symmetrical molecule is bent by 14°, with potassium situated 2.58 Å below the plane of the SeNSe donors. The structural variations between the two independent molecules of **9** point to low energy barriers for backbone bending and the lateral displacement of the potassium cation relative to the Se donors. The sum of the C–Se–C and C–Se–K bond angles is 304° and 318° (in the more symmetrical molecule) and 304° and 326° (in the less symmetrical molecule). Compounds **9** and **6** are only the second and third structurally authenticated examples of complexes containing potassium–selenoether interactions.

In telluroether compound **10**, the K–Te distances are 3.808(1) Å and 3.916(1) Å.‡ The difference between the average K–Te distance in **10** (3.862 Å) and the average K–Se distance in **9** (3.469 Å) is 0.393 Å, which is significantly larger than the difference between the covalent radii of Se and Te (0.18 Å)[42], suggestive of a weaker (*vide infra*) K–E interaction in the telluroether compound. The tellurium atoms in **10** are more strongly pyramidalized than the selenium atoms in **9**, with the sum of the C–Te–C and C–Te–K angles equal to 291° and 304°. The K–N distance is 2.842(3) Å, and the K–O distances range from 2.660(3) to 2.865(3) Å.§ According to SHAPE analysis, the arrangement of the donors around potassium is best described as a distorted capped trigonal prism, with O(4) as the capping atom. The ATe_2^{Tripp2} ligand backbone is slightly bent (by 7°), and the potassium cation sits 2.80 Å below the plane of the TeNTe donors.

Solution NMR spectroscopy

Although compounds **3** and **4** are dimers in the solid-state, ^{1}H and ^{13}C{^{1}H} NMR spectra in toluene-d_8 contain only two methyl signals, indicative of ligand top-bottom and side-to-side symmetry on the NMR timescale. The proton and carbon resonances associated with the C*Me*$_2$ group in **3** and **4** are also broadened relative to other signals at room temperature. These data are consistent with rapid dissociation/re-association of the dimer on the NMR timescale, and upon cooling a toluene-d_8 solution of **4** to –68 °C, the C*Me*$_2$ peak decoalesced into two signals integrating to three protons each, as expected for the dimeric structure (Figure S9). Compounds **3** and **4** gave rise to broad room temperature ^{7}Li NMR signals at 3.30 and 4.38 ppm, respectively.

In contrast to lithium compounds **3** and **4**, potassium compounds **5** and **6** are poorly soluble in C_6D_6, so NMR spectra were obtained in THF-d_8 (for **5**) or C_6D_6 containing a drop of dme (for **6**). These spectra indicate apparent C_{2v} symmetry in solution. Similarly, ^{1}H and ^{13}C{^{1}H} NMR spectra of more soluble **7**-**10** in C_6D_6 are consistent with C_{2v} symmetry on the NMR timescale. The apparent C_{2v} symmetry of monomeric **6**, **9** and **10** imply that potassium is able to migrate rapidly between coordination sites above and below the plane of the ligand backbone (assuming that potassium remains coordinated to the ligand; *vide infra*). Additionally, while two signals would be expected for the diastereotopic *ortho*-isopropyl methyl groups in **9** and **10**, only a single resonance was observed in the ^{1}H and ^{13}C{^{1}H} NMR spectra, indicative of rapid rotation of the 2,4,6-triisopropylphenyl groups on the NMR timescale. This process is presumably facilitated by the long chalcogen–carbon and chalcogen–potassium bonds and acute C–E–C angles which minimize steric hindrance. Potassium was shown to be substantially coordinated to the ASe_2^{Ph2} and ASe_2^{Tripp2} ligands in C_6D_6 solutions of **6** and **9**, respectively, given that the addition of 2,2,2-cryptand produced significant shifts in the ^{1}H NMR resonances for the chalcogenoether-containing ligands (accompanied by 2,2,2-cryptand ^{1}H NMR resonances shifted relative to those of the free cryptand). The ^{77}Se NMR resonance for **9** also shifted to higher frequency by 30 ppm upon addition of 2,2,2-cryptand (Figures S12, S22 and S23; products formed from reactions of **6** and **10** with 2,2,2-cryptand in C_6D_6 were insufficiently soluble for ^{77}Se (for **6**) or ^{1}H and ^{125}Te (for **10**) NMR signals to be observed, even after addition of small amounts of THF or dme).

For compounds **2**-**4** and **6**-**10**, ^{77}Se{^{1}H}, ^{125}Te{^{1}H}, and/or ^{7}Li NMR spectra were obtained in C_6D_6 (with a small amount of added dme in the case of **6**), and chemical shift values are provided in Table 1. All resonances (*vide infra*) appeared as singlets, with no discernable coupling.

The ^{77}Se NMR chemical shifts for pro-ligands **2** and **7** are 295 and 162 ppm, falling within the expected range for diarylselenide compounds, considering the sterically hindered and electron donating substituents on the aryl rings attached to selenium. For comparison, the ^{77}Se NMR chemical shifts for $SePh_2$,[43] $Se(C_6H_4NH_2\text{-}p)_2$,[44] PhSeMes,[45] $SeMes_2$ and $SeTrip_2$[43] are 416, 378, 289, 225 and 162 ppm, respectively. The ^{77}Se NMR resonances for potassium compounds **6** and **9** are shifted to high frequency relative to pro-ligands **2** and **7**, by 62 and 41 ppm, respectively. By contrast, the ^{77}Se NMR chemical shift for $[Li(ASe_2^{Ph2})]_2$ (**4**) is 283 ppm, which is 12 ppm lower frequency than pro-ligand **2**. ^{77}Se NMR chemical shifts were not reported for the previously described s-block selenoether compounds (sodium, potassium,[6] magnesium,[25] calcium, strontium[24, 25] and bari-

um[25] complexes of [18]aneO$_4$Se$_2$; *vide supra*). However, coordination of [18]aneO$_4$Se$_2$ to diamagnetic rare earth ions produced shifts to either high or low frequency. For example, a small high frequency shift was observed upon complexation of [18]aneO$_4$Se$_2$ (^{77}Se δ 140 ppm) to scandium to form [ScCl$_2$([18]aneO$_4$Se$_2$)][FeCl$_4$] (^{77}Se δ 150 ppm). By contrast, ^{77}Se NMR chemical shifts of 103, 108, 125 and 137.5 ppm were reported for [YCl$_2$([18]aneO$_4$S$_2$)][FeCl$_4$], [LuI$_2$([18]aneO$_4$Se$_2$)]I, [YI$_2$([18]aneO$_4$Se$_2$)]I, and [LaI$_3$([18]aneO$_4$Se$_2$)], respectively.[46]

The ^{125}Te NMR chemical shift for H[ATe$_2^{Tripp2}$] (**8**) is 197 ppm, which is higher frequency than the ^{77}Se chemical shift for the selenium analogue (**7**; 162 ppm), as is typical for isostructural selenoether and telluroether compounds.[47] For comparison, reported ^{125}Te NMR chemical shifts for TePh$_2$,[48] TeMes$_2$ and TeTripp$_2$[49] are 685, 276 and 175 ppm, respectively. Upon deprotonation of **8** to form [K(ATe$_2^{Tripp2}$)(dme)$_2$] (**10**), the ^{125}Te resonance shifted to high frequency by 34 ppm. This trend matches that observed for the ^{77}Se NMR chemical shift of potassium complex **9** relative to pro-ligand **7**.

Table 1. ^{77}Se, ^{125}Te and/or ^{7}Li NMR chemical shifts (ppm) for compounds **2**-**4** and **6**-**10** in C$_6$D$_6$ (with added dme in the case of **6**) All resonances are from 1D ^{77}Se{^{1}H}, ^{125}Te{^{1}H} or ^{7}Li NMR spectra and appeared as singlets with no discernible coupling.

Compound	δ ^{77}Se	δ ^{125}Te	δ ^{7}Li
H[ASe$_2^{Ph2}$] (**2**)	295.39	–	–
[Li(AS$_2^{Ph2}$)]$_2$ (**3**)	–	–	3.30
[Li(ASe$_2^{Ph2}$)]$_2$ (**4**)	283.43	–	4.38
[K(ASe$_2^{Ph2}$)(dme)$_2$] (**6**)	357.02	–	–
H[ASe$_2^{Tripp2}$] (**7**)	162.15	–	–
H[ATe$_2^{Tripp2}$] (**8**)	–	196.86	–
[K(ASe$_2^{Tripp2}$)(dme)$_2$] (**9**)	203.30	–	–
[K(ATe$_2^{Tripp2}$)(dme)$_2$] (**10**)	–	230.72	–

DFT calculations

DFT calculations (ADF, gas-phase, all-electron, PBE, D3-BJ, TZ2P, ZORA) were performed on **3**, **4**, **6**, **9** and **10** in order to gain insight into the nature of the alkali metal–chalcogenoether interactions. For complexes **9** and **10**, models were used in which the 2,4,6-triisopropylphenyl substituents have been replaced by 2,6-diisopropylphenyl (Dipp) groups: [K(ATe$_2^{Dipp2}$)(dme)$_2$] (**9***) and [K(ATe$_2^{Dipp2}$)(dme)$_2$] (**10***).

Compounds **4** and **6** converged to geometries which are a close match to the X-ray crystal structures, with M–N and M–Se distances within 0.06 Å of the crystallographic values. Lithium dimer **3** also converged to a structure with Li–S and Li–N distances that are within 0.03 Å of experimental values, although one monomer unit is skewed relative to the other, resulting in C_2 symmetry with a Li–N–Li–N dihedral angle of 11° (compared to the crystallographically observed dihedral angle of 0°). When C_{2v} symmetry was imposed, the resulting structure (which matches closely with the crystal structure) was found to be higher in energy by just 7 kJ mol^{-1}, suggesting that the geometry in the X-ray structure arises due to crystal packing. The Li–S and Li–N distances in the two calculated geometries of **3** are within 0.01 Å of one another and the ligand bend angles are identical (Table S1), so the C_2-symmetric energy minimum was used in all subsequent discussion.

In **9*** and **10***, the K–E distances are underestimated by 0.07-0.14 Å or 0.01-0.28 Å for **9*** (relative to the two independent molecules in the unit cell of **9**) and by 0.19 and 0.21 Å in **10***. Furthermore, the K–N distances are overestimated by 0.12 Å or 0.16 Å in **9***, and underestimated by 0.04 Å in **10***. Optimization of **9*** with K–Se and K–N distances constrained to crystallographic values yielded **9*$_{Constr}$**¶ which is just 5 kJ mol^{-1} higher in energy than **9***. Similarly, optimization of **10*** with the K–Te distances constrained to crystallographic values afforded a structure (**10*$_{Constr}$**; with a K–N distance that is within 0.04 Å of the experimental value) that is only 6 kJ mol^{-1} higher in energy than **10***. This is indicative of a shallow energy minimum for modest changes in the K–N and K–E distances in **9** and **10**.

Quantum Theory of Atoms in Molecules (QTAIM) bond critical points (BCPs) were located between the alkali metal cations and each of the chalcogen donors in **3**, **4**, **6**, **9***, **9*$_{Constr}$** and **10***, supporting the presence of alkali metal–chalcogenoether interactions. These interactions are predominantly electrostatic, as evidenced by small bond delocalization index (δ_{M-E}) values of 0.03-0.08, and positive values for the total energy density of Cremer and Kraka (H_b) at the BCPs (0.001-0.003; Table 2). By contrast, K–Te bond critical points were not observed for **10*$_{Constr}$**, where the K–Te distances have been constrained to match those in the X-ray crystal structure. This suggests that K–Te interactions are significant in some but not all structures on the shallow energy surface associated with modest changes in the K–N and K–Te distances. The positive H_b values for the M–E bonds in **3**, **4**, **6**, **9***, **9*$_{Constr}$** and **10*** contrast the negative H_b values for the U–E bonds in the uranium(IV) complexes [(AS$_2^{Ph2}$)$_2$UI$_2$] and [(ASe$_2^{Ph2}$)$_2$UI$_2$],[41] illustrating the more electrostatic nature of the alkali metal chalcogenoether interactions.

For all structures in Table 2, Natural Bond Order (NBO) analysis revealed alkali metal orbital contributions of less than 3 % to the Natural Localized Molecular Orbitals (NLMOs) with an appropriate orientation to be involved in M–E bonding ("LP-1"; Table S2). Nevertheless, lithium complexes **3** and **4** feature higher metal orbital contributions (1.2-1.4 % for **3** and 2.4-2.7 % for **4**) to the metal–chalcogen interactions, compared to potassium structures **6**, **9***, **9*$_{Constr}$**, **10*** and **10*$_{Constr}$** (0.2-0.6 %), suggestive of somewhat increased covalency. Furthermore, greater lithium orbital contributions to the E NLMOs were observed for the Li–Se interactions in **4** relative to the Li–S interactions in **3** (by ~1.3%). This increase, while small, is in line with the trend observed for [(AS$_2^{Ph2}$)$_2$UI$_2$] and [(ASe$_2^{Ph2}$)$_2$UI$_2$], where an increase in uranium orbital involvement (from 9.9-14.4 % in the former to 11.4-16.6 % in the latter) was observed.[41] These trends are echoed in the M–E Mayer bond orders (Table 2), which are 0.26-0.27 and 0.28-0.29 in lithium compounds **3** and **4**, respectively, 0.07-0.13 in potassium selenoether compounds **6** and **9***, and 0.07 or less in potassium selenoether structure **9*$_{Constr}$** and telluroether structures **10*** and **10*$_{Constr}$**, suggestive of (a) increased covalency in the lithium compounds relative to the potassium compounds, (b) marginally increased covalency in the Li–SeR$_2$ interactions in **4** relative to the Li–SR$_2$ interactions in **3**, and (c) marginally decreased covalency in the K–TeR$_2$ interactions relative to the K–SeR$_2$ interactions. Nevertheless, the H_b and δ_{M-E} metrics do not follow the same trends, highlighting the challenges associated with probing small differences in covalency in highly ionic interactions.

Table 2. Computational data for **3**, **4**, **6**, **9***, **10*** and **10*$_{Constr}$** (M = Li or K; E = S, Se or Te): QTAIM bond delocalization index (δ) and the total energy density of Cremer and Kraka (H_b) at the bond critical point (bcp), % metal contribution to the NLMO with an appropriate orientation to be involved in M–E bonding (normalized to include only metal and chalcogen contributions), and Mayer bond orders (B.O.). Individual data or data ranges are for all of a particular type of bond in the structure (i.e. they are not averaged values).

Compound	δ(M–E) ($\times 10^{-2}$)	H_b(M–E) ($\times 10^{-3}$)	% M in E NLMO (LP-1)[a]	M–E Mayer B.O.	M–O Mayer B.O.	M–N Mayer B.O.
$[Li(AS_2^{Ph2})]_2$ (**3**)	5.9-6.2	3.0	1.2-1.4	0.26-0.27	N/A	0.14-0.25
$[Li(ASe_2^{Ph2})]_2$ (**4**)	7.0-7.2	2.3-2.4	2.4-2.7	0.28-0.29	N/A	0.15-0.20
$[K(ASe_2^{Ph2})(dme)_2]$ (**6**)	7.9-8.4	1.3-1.4	0.5	0.11-0.13	<0.05	<0.05
$[K(ASe_2^{Dipp2})(dme)_2]$ (**9***)	7.5	1.3	0.2-0.3	0.07-0.10	<0.05 & 0.07	<0.05
$[K(ASe_2^{Dipp2})(dme)_2]$ with constraint (**9*$_{Constr}$**)	5.6-6.4	1.3	0.2-0.3	<0.05 & 0.06	<0.05 & 0.07	<0.05
$[K(ATe_2^{Dipp2})(dme)_2]$ (**10***)	5.1-5.9	1.0-1.2	0.5-0.6	0.06-0.07	<0.05 & 0.06	<0.05
$[K(ATe_2^{Dipp2})(dme)_2]$ with constraint (**10*$_{Constr}$**)	3.0-4.3	no BCP	0.5-0.6	<0.05	<0.05 & 0.05-0.06	<0.05

[a] LP-1 denotes the E-based NLMO with the most appropriate orientation for involvement in M–E bonding.

SUMMARY AND CONCLUSIONS

The rigid phenyl-substituted thioether and selenoether-containing pro-ligands $H[AS_2^{Ph2}]$ (**1**) and $H[ASe_2^{Ph2}]$ (**2**), and new bulky 2,4,6-triisopropylphenyl-substituted selenium and tellurium analogues, $H[ASe_2^{Tripp2}]$ (**7**) and $H[ATe_2^{Tripp2}]$ (**8**), were employed to generate a series of lithium and potassium chalcogenoether complexes. In the solid-state, the lithium compounds, $[Li(AE_2^{Ph2})]_2$ (E = S (**3**), Se (**4**)) are dimers, whereas $[K(AS_2^{Ph2})(dme)]_x$ (**5**) is a 1-dimensional polymer, and $[K(ASe_2^{Ph2})(dme)_2]$ (**6**) and $[K(AE_2^{Tripp2})(dme)_2]$ (E = Se (**9**), Te (**10**)) are monomers. The solution ^{77}Se and ^{125}Te NMR resonances for potassium compounds **6**, **9** and **10** are shifted to high frequency relative to pro-ligands **2**, **7** and **8** (by 62, 41 and 34 ppm, respectively). By contrast, the ^{77}Se NMR chemical shift for $[Li(ASe_2^{Ph2})]_2$ (**4**) is 12 ppm lower frequency than that of pro-ligand **2**. Selenoether compounds **6** and **9** are only the second and third complexes containing potassium–selenoether bonds, while **4** is the first lithium–selenoether complex.

For complex **10**, changes in the K–Te and K–N distances were shown by DFT calculations to lie on a shallow potential energy surface, providing access to structures with and without significant K–Te interactions; K–Te interactions are evident in the DFT-calculated energy minimum, whereas QTAIM calculations on a structure in which the K–Te distances have been constrained to match those in the X-ray crystal structure did not show a bond critical path between potassium and tellurium.

DFT and QTAIM calculations are consistent with highly ionic interactions between the alkali metals and soft chalcogenoether donors. Nevertheless, trends in the Mayer bond orders and % alkali metal contributions to NLMOs with an appropriate orientation to be involved in M–E (E = S, Se or Te) bonding suggest somewhat increased covalency in the lithium compounds relative to the potassium compounds, and perhaps also marginally increased covalency in the Li–SeR_2 versus Li–SR_2 interactions, and K–SeR_2 versus K–TeR_2 interactions.

EXPERIMENTAL SECTION

General Details: An argon-filled MBraun UNIlab glove box equipped with a –30 °C freezer was employed for the manipulation and storage of all oxygen- and moisture- sensitive compounds. Air-sensitive reactions were performed on a double-manifold high-vacuum line equipped with an Edwards RV 12 vacuum pump using standard techniques. ^{n}BuLi solution (1.6 M in hexanes), and 1,2-dimethoxyethane (dme) were purchased from Sigma Aldrich. 4,5-dibromo-2,7,9,9-tetramethylacridan ($H[ABr_2]$)[39], bis(2,4,6-triisopropylphenyl) diselenide (Se_2Tripp_2)[50], $H[AS_2^{Ph2}]$[41], $H[ASe_2^{Ph2}]$[41], KCH_2Ph[51], $[K(AS_2^{Ph2})(dme)]$[41], $[K(ASe_2^{Ph2})(dme)_2]$[41] were synthesized following previously reported procedures. Bis(2,4,6-triisopropylphenyl) ditelluride (Te_2Tripp_2) was prepared following a modification of the literature procedure for the synthesis of Se_2Tripp_2 (see supplementary information). 2,4,6-triisopropylphenyl bromide and 2,2,2-crytpand were purchased from Sigma Aldrich, dried over 4 Å molecular sieves (as a solution in Et_2O in the case of 2,2,2-cryptand) for one week, degassed, and either centrifuged or filtered through a celite plug to remove sieve powder before use. Reactions of $H[ASe_2^{Ph2}]$ with KCH_2Ph or $H[AS_2^{Ph2}]$ with KH or KCH_2Ph in toluene at 60 °C generated precipitates that were only soluble in donor solvents such as THF and dme. Reactions to prepare sodium, rubidium or caesium salts of the ligands were not attempted.

Hexanes, toluene, and Et_2O were purchased from Caledon, and deuterated solvents were purchased from Cambridge Isotope Laboratories, Inc. Hexanes, Et_2O and toluene were initially dried and distilled at atmospheric pressure from sodium/benzophenone (Hexanes, Et_2O) and sodium (toluene). 1,2-dimethoxyethane (dme) was initially dried over 4 Å molecular sieves, followed by further drying over Na/Ph_2CO before being distilled for use. All solvents were stored over an appropriate drying agent (Et_2O, toluene, 1,2-dimethoxyethane (dme), C_6D_6, toluene-d_8 = Na/Ph_2CO; hexanes = Na/Ph_2CO/tetraglyme) and introduced to reactions or air-free solvent storage flasks via vacuum transfer with condensation at –78 °C. Argon gas was purchased from Air Liquide.

^{1}H, ^{13}C{^{1}H}, ^{7}Li, ^{77}Se{^{1}H}, and ^{125}Te{^{1}H} NMR spectra of all air-sensitive samples were acquired at room temperature in J-Young tubes on either a Bruker AV-600 MHz or AV-500 MHz spectrometer. ^{1}H and ^{13}C{^{1}H} spectra were referenced relative to the residual proteo signals of the solvent (C_6D_6 or toluene-d_8) or the solvent carbon resonances respectively (C_6D_6: ^{1}H = 7.16 ppm; ^{13}C = 128.06 ppm / toluene-d_8: ^{1}H = 7.09, 7.01, 6.97, 2.08 ppm; ^{13}C = 137.48, 128.87, 127.96, 125.13, 20.43 ppm). ^{7}Li, ^{77}Se{^{1}H} and ^{125}Te{^{1}H} spectra were referenced by indirect referencing from a ^{1}H NMR spectrum.[52] Peak assignments in the spectra of all new diamagnetic compounds were made with the aid of DEPT-q, COSY, HSQC and HMBC experiments.

X-ray crystallographic analyses were performed with suitable crystals coated in paratone oil on either a STOE IPDS II diffractometer equipped with a 3 kW sealed tube Mo generator or a Bruker Dual Source D8 Venture diffractometer using the IμS 3.0 Mo source at 70 watts with a HELIOS Mo focusing optic (ELM33) in the McMaster Analytical X-Ray (MAX) Diffraction Facility. Data was processed with OLEX 2[53] and solved by intrinsic (SHELXT)[54] methods. Structure refinement was performed with SHELXL[55] in OLEX 2. In the structure of **9**·0.5 hexane, hexane was badly disordered and could not be satisfactorily modelled and was therefore treated with the BYPASS method.[56] Images were rendered using Ortep3 and POV-Ray.

Combustion elemental analyses were carried out at Midwest Microlabs, the University of Calgary, or McMaster University.

DFT Details: Geometry optimization calculations were conducted with ADF within the AMS DFT package (SCM, version 2021.104 or 2022.103).[57] Calculations were performed in the gas phase within the generalized gradient approximation using the 1996 Perdew-Burke-Ernzerhof exchange and correlation functional (PBE),[58] using the scalar zeroth-order regular approximation (ZORA)[59-63] for relativistic effects, and Grimme's DFT-D3-BJ dispersion correction.[64, 65] These calculations were conducted using all-electron triple-ζ basis sets with two polarization functions (TZ2P) and fine integration grids (Becke[66, 67] verygood-quality) with default convergence criteria for energy and gradients. Analytical frequency calculations[68-70] were conducted to ensure that each geometry optimization led to an energy minimum. Quantum Theory of Atoms in Molecules (QTAIM)[71] properties were obtained using the QTAIM keyword[57] with an analysis level of Full[72-79] (QTAIM calculations were also performed on a single point calculation of **10*$_{Constr}$**, with a Becke integration grid quality of "Excellent", but did not find BCPs between potassium and tellurium), and NBO analysis[80] was carried out using NBO 6.0 within the AMS DFT package.

Lithium 4,5-bis(phenylsulfido)-2,7,9,9-tetramethylacridanide {[Li(AS$_2^{Ph2}$)]$_2$} (3): A solution of H[AS$_2^{Ph2}$] (342.4 mg, 0.7548 mmol) in hexanes (~30 ml) was cooled to –78 °C, and 1.1 equiv. of 1.6 M ^{n}BuLi in hexanes (0.9057 mmol) was added dropwise to the yellow mixture under a heavy flow of argon, producing a pale-green precipitate. The reaction was allowed to stir at –78 °C for two hours, after which the cooling bath was removed. Upon warming for 20 minutes, the precipitate turned orange and the solution was evaporated to dryness *in vacuo*, yielding **3** as an orange powder in 98 % yield (340 mg). The solid can be stored indefinitely at –30 °C in an argon atmosphere. X-ray quality crystals were obtained by preparing a concentrated toluene solution, addition of a couple of drops of benzene, and cooling at –30 °C for two weeks. **^{1}H NMR (C$_6$D$_6$, 600 MHz):** δ 7.42 (s, 2H, AcridanC*H*), 7.30 (s, 2H, AcridanC*H*), 6.65-6.64 (d, $J_{H\text{-}H}$ 7.4 Hz, 4H, *o*-Ar*H*), 6.49-6.44 (m, 6H, *m*,*p*-Ar*H*), 2.19 (s, 6H, C*Me*), 1.72 (s, 6H, C*Me$_2$*). **^{13}C{^{1}H} NMR (C$_6$D$_6$, 150 MHz):** δ 152.93 (Acridan*C*Me), 136.52 (Ar*C*S), 135.57 (Acridan*C*H), 134.53 (Acridan*C*), 129.06 (*o*-Ar*C*H), 127.90 (Acridan*C*H), 127.17 (Acridan*C*N), 126.54 (*m*-Ar*C*H), 125.51 (*p*-Ar*C*H), 117.55 (Acridan*C*S), 37.86 (Acridan*C*Me$_2$), 29.37 (C*Me$_2$*), 20.91 (Acridan*C*H$_3$). **^{7}Li NMR (C$_6$D$_6$, 194 MHz):** δ 3.30 (br s). **Anal. Calcd for C$_{29}$H$_{24}$NS$_2$Li:** C, 75.79; H, 5.71 ; N, 3.05%. **Found:** C, 75.21; H, 6.11; N 3.74%.

Lithium 4,5-bis(phenylselenido)-2,7,9,9-tetramethylacridanide {[Li(ASe$_2^{Ph2}$)]$_2$} (4): A solution of H[ASe$_2^{Ph2}$] (201.8 mg, 0.3686 mmol) in hexanes (~20 ml) was cooled to –78 °C and 1.1 eq. of 1.6M ^{n}BuLi in hexanes (0.25ml, 0.4055 mmol) was added dropwise to the stirring yellow solution, converting it into a pale yellowish-green suspension. The reaction was stirred at –78 °C for 10 minutes and then allowed to stir at room temperature for 2 hours, during which time the pale yellow-green suspension slowly became light orange. Volatiles were removed *in vacuo* for 2 hours, affording 182.4 mg of **4** (89 %) as a light orange powder. The solid can be stored indefinitely at –30 °C in an argon atmosphere. X-ray quality crystals were obtained from a concentrated toluene solution cooled to –30 °C for three days. **^{1}H NMR (C$_6$D$_6$, 500 MHz):** δ 7.46 (s, 2H, AcridanC*H*), 7.43 (s, 2H, AcridanC*H*), 6.76-6.75 (d, $J_{H\text{-}H}$ 7.8 Hz, 4H, *o*-Ar*H*), 6.55-6.52 (m, 4H, *p*-Ar*H*), 6.45-6.41 (m, 4H, *m*-Ar*H*), 2.18 (s, 6H, C*Me*), 1.76 (s, 6H, C*Me$_2$*). **^{13}C{^{1}H} NMR (C$_6$D$_6$, 125 MHz):** δ 153.17 (Acridan*C*Me), 137.57 (Acridan*C*H), 134.52 (Acridan*C*), 132.05 (Ar*C*Se), 129.29 (*m*-Ar*C*H), 129.00 (*o*-Ar*C*H), ~128 (Acridan*C*H), ~128 (Acridan*C*N), 126.08 (*p*-ArCH), 117.27 (Acridan*C*Se), 38.16 (Acridan*C*Me$_2$), 29.62 (*C*H$_3$), 20.79 (*C*H$_3$). **^{77}Se{^{1}H} NMR (C$_6$D$_6$, 114 MHz):** δ 2.83.43 (s). **^{7}Li NMR (C$_6$D$_6$, 194 MHz):** δ 4.38 (br s). **Anal. Calcd for C$_{29}$H$_{24}$NSe$_2$Li:** C, 62.94; H, 4.74; N, 2.53%. **Found:** C, 63.78; H, 4.80; N, 2.37%.

4,5-bis(2,4,6-triisopropylphenylselenido)-2,7,9,9-tetramethylacridan (H[ASe$_2^{Tripp2}$]) (7): H[ABr$_2$] (500 mg, 1.27 mmol) was charged to a 2-neck round-bottom flask and dissolved in ~25 ml of Et$_2$O. A glass stopper was outfitted on one of the necks and a distillation apparatus was outfitted on the other. The apparatus was appended to a vacuum line and the mixture was stirred at room temperature under argon until the H[ABr$_2$] was completely dissolved. The solution was then cooled to –78 °C and 3 eq. of 1.63 M ^{n}BuLi in hexanes (2.33ml, 3.80 mmol) was added dropwise while stirring, producing a light yellow solution. The cold bath was removed, and the reaction was left to stir at room temperature for 2 hours, after which the solution was cooled again to –78 °C and 2 eq. of Se$_2$Tripp$_2$ (1.43 g, 1.27 mmol) dissolved in ~10 ml of Et$_2$O was added dropwise to the reaction, turning the solution orange. The reaction was left to stir under argon with the cold bath up overnight, which slowly warmed, allowing the reaction to come to room temperature over several hours. The orange reaction mixture was then quenched with 1 eq. of 1 M HCl$_{(aq)}$ (3.80 ml, 3.80 mmol) while stirring vigorously, producing copious amounts of white precipitate which redissolved over time, and then allowed to continue stirring for 10 minutes under argon. Volatiles were removed under vacuum, leaving behind an orange waxy residue. The receiving flask on the distillation apparatus was then cooled to –78 °C and HSeTripp, ^{n}BuSeTripp and Se$_2$Tripp$_2$ were distilled from the reaction flask by maintaining it at 130 °C under vacuum for 5 hours (a heat gun was occasionally used to help the by-products transfer from the distillation arm into the receiving flask). Once orange Se$_2$Tripp$_2$ stopped collecting in the neck of the distillation apparatus, the flask was removed from the vacuum line and the residues were dissolved in ~30 ml of Et$_2$O and washed with 2 x 75 ml NaHCO$_3$ in air. The organic layer was collected, dried over MgSO$_4$ and gravity filtered into a 50 ml round bottom flask and evaporated to dryness under vacuum. The flask was outfitted with a sublimation apparatus and the residues were sublimed at 140 °C to drive off remaining Se$_2$Tripp$_2$ as an orange residue on the cold finger. The Se$_2$Tripp$_2$ was washed off the cold finger, and the sublimation was continued at 160 °C for ~3 hours. This afforded **7** as an off-white solid, which was collected (155 mg) in 15 % yield. **^{1}H NMR (C$_6$D$_6$, 500 MHz):** δ 8.53 (s, 1H, N*H*), 7.19 (s, 4H, Ar*H*), 7.02 (s, 2H, Acridan*H*), 7.01 (s, 2H, Acridan*H*), 4.26-4.18 (sept, $J_{H\text{-}H}$ 6.45 Hz, *o*-C*H*Me$_2$), 2.78-2.70 (sept, $J_{H\text{-}H}$ 7.04 Hz, *p*-C*H*Me$_2$), 1.91 (s, 6H, C*Me$_2$*), 1.51 (s, 6H, C*Me*), 1.28-1.27 (d, $J_{H\text{-}H}$ 7.04 Hz, 24H, *o*-CH*Me$_2$*), 1.16-1.15 (d, $J_{H\text{-}H}$ 7.04 Hz, 12H, *p*-CH*Me$_2$*). **^{13}C{^{1}H} NMR (C$_6$D$_6$, 125 MHz):** δ 153.71 (*o*-Aryl*C*), 150.60 (*p*-Aryl*C*), 136.50 (Acridan*C*N), 131.15 (Acridan*C*H), 130.71 (Acridan*C*), 130.08 (Acridan*C*Me), ~128 (Aryl*C*Se), 124.91 (Acridan*C*H), 122.69 (Aryl*C*H), 118.88 (Acridan*C*Se), 37.59 (Acridan*C*Me$_2$), 34.99 (*o*-*C*HMe$_2$), 34.58 (*p*-*C*HMe$_2$), 30.04 (C*Me*), 24.68 (*o*-CH*Me$_2$*), 24.08 (*p*-CH*Me$_2$*), 20.84 (C*Me$_2$*). **^{77}Se{^{1}H} NMR (C$_6$D$_6$, 95 MHz):** δ 162.15 (s). **Anal. Calcd for C$_{47}$H$_{63}$NSe$_2$:** C, 70.57; H, 7.94; N, 1.75%. **Found:** C, 70.49; H, 8.13; N, 1.71%.

4,5-bis(2,4,6-triisopropylphenyltellurido)-2,7,9,9-tetramethylacridan (H[ATe$_2^{Tripp2}$]) (8): H[ABr$_2$] (199.5mg, 0.5049 mmol) was charged to a 2-neck round-bottom flask and dissolved in ~20 ml of Et$_2$O. A glass stopper was outfitted on one of the necks and a distillation apparatus was outfitted on the other. The apparatus was appended to a vacuum line and the H[ABr$_2$] was stirred at room temperature under argon until completely dissolved. The solution was then cooled to –78 °C and 3 eq. of 1.63 M ^{n}BuLi in hexanes (0.93ml, 1.5 mmol) was added dropwise while stirring, producing a light yellow solution. The cold bath was removed, and the reaction was left to stir at room temperature for 2 hours, after which the solution was cooled again to –78 °C and 2 eq. of Te$_2$Tripp$_2$ (570.2 mg, 1.010 mmol) dissolved in ~10 ml of Et$_2$O was added dropwise to the reaction, turning the solution red-orange. The reaction was covered with aluminum foil to protect it from light and left to stir under argon with the cold bath up overnight, which slowly warmed, allowing the reaction to come to room temperature over several hours. The foil was removed, and the orange reaction mixture was then quenched with 1 eq. of 1 M HCl$_{(aq)}$ (1.51 ml, 1.51 mmol) while stirring vigorously, producing copious amounts of white precipitate which redissolved over time, and then allowed to continue stirring for 10 minutes under argon. Volatiles were removed under vacuum, affording a dark red waxy residue. The receiving flask on the distillation apparatus was then cooled to –78 °C and HTeTripp, ^{n}BuTeTripp and Te$_2$Tripp$_2$ were distilled from the reaction flask at 155 °C under vacuum for 4 hours (a heat gun was occasionally used to help the by-products transfer from the distillation arm into the receiving flask). Once red Te$_2$Tripp$_2$ stopped collecting in the neck of the distillation apparatus, the flask was removed from the vacuum line and the residues were dissolved in ~20 ml of Et$_2$O and washed with 2 x 75 ml NaHCO$_3$ in air. The organic layer was collected, dried over MgSO$_4$, gravity filtered into a 50 ml round bottom flask, and evaporated to dryness under vacuum. The flask was outfitted with a sublimation apparatus and the residues were sublimed at 150 °C to drive off remaining Te$_2$Tripp$_2$ as a red residue on the cold finger. The Te$_2$Tripp$_2$ was washed

off the cold finger, and the sublimation was continued at 170 °C for ~2 hours to afford **8** as an off-white pink-orange solid which was collected (140 mg) in 21 % yield. **^{1}H NMR (C_6D_6, 600 MHz):** δ 8.43 (s, 1H, *N*H), 7.48 (s, 2H, AcridanC*H*), 7.15 (s, 4H, ArC*H*), 7.06 (s, 2H, AcridanC*H*), 4.19-4.12 (sept, $J_{H\text{-}H}$ 6.80 Hz, 4H, *o*-C*H*Me$_2$), 2.76-2.69 (sept, $J_{H\text{-}H}$ 6.80 Hz, 2H, *p*-C*H*Me$_2$), 1.92 (s, 6H, C*Me*), 1.49 (s, 6H, C*Me$_2$*), 1.26-1.25 (d, $J_{H\text{-}H}$ 6.87 Hz, 24H, *p*-CH*Me$_2$*), 1.15-1.14 (d, $J_{H\text{-}H}$ 6.93 Hz, 12H, *o*-CH*Me$_2$*). **^{13}C{^{1}H} NMR (C_6D_6, 150 MHz):** δ 155.22 (*o*-Aryl*C*), 150.71 (*p*-Aryl*C*), 139.83 (Acridan*C*Te), 138.53 (Acridan*C*H), 131.31 (Acridan*C*Me), 129.80 (Acridan*C*), 126.39 (Acridan*C*H), 122.26 (Aryl*C*H), 121.59 (Aryl*C*Te), 104.03 (Acridan*C*N), 40.40 (*o*-*C*HMe$_2$), 37.92 (*C*Me$_2$), 34.47 (*p*-*C*HMe$_2$), 29.66 (C*Me$_2$*), 24.95 (*o*-CH*Me$_2$*), 24.12 (*p*-CH*Me$_2$*), 20.61 (C*Me*). **^{125}Te{^{1}H} NMR (C_6D_6, 189 MHz):** δ 196.86 (s) **Anal. Calcd for $C_{47}H_{63}NTe_2$:** C, 62.92; H, 7.08; N, 1.56 %. **Found:** C, 63.20; H, 7.41; N, 1.53 %.

Potassium 4,5-bis(2,4,6-triisopropylphenylselenido)-2,7,9,9-tetramethylacridanide · 2 dme {[K(ASe$_2^{Tripp2}$)(dme)$_2$]} (9): H[ASe$_2^{Tripp2}$] (250 mg, 0.313 mmol) and 1.2 eq. KCH$_2$Ph (48.8 mg, 0.375 mmol) were charged to a 50 ml round-bottom flask and then dissolved in ~20 ml of dme. The flask was appended to a vacuum line and immediately stirred, turning the solution from orange to bright yellow. The reaction was stirred at room temperature under argon for 15 minutes, after which the volatiles were removed *in vacuo* and the residues dried for 20 minutes, leaving a glassy orange film. The flask was brought into the glovebox and 281 mg of orange-yellow [K(ASe$_2^{Tripp2}$)(dme)$_2$] was collected (88 % yield). The solid can be stored for at least one year at –30 °C in an argon atmosphere. X-ray quality crystals were grown from dme/hexanes over 2 weeks at –30 °C. **^{1}H NMR (C_6D_6, 500 MHz):** δ 7.33 (s, 4H, ArC*H*), 7.06 (s, 2H, AcridanC*H*), 6.43 (s, 2H, AcridanC*H*), 4.03-3.96 (sept, $J_{H\text{-}H}$ 6.86 Hz, 4H, *o*-C*H*Me$_2$), 3.12 (s, 8H, OC*H$_2$*), 2.98 (s, 12H, O*Me*), 2.90-2.84 (sept, $J_{H\text{-}H}$ 6.98 Hz, 2H, *p*-C*H*Me$_2$), 2.10 (s, 6H, C*Me*), 1.78 (s, 6H, C*Me$_2$*), 1.31-1.30 (d, $J_{H\text{-}H}$ 6.74 Hz, 24H, *o*-CH*Me$_2$*), 1.27-1.26 (d, $J_{H\text{-}H}$ 6.87 Hz, 12H, *p*-CH*Me$_2$*). **^{13}C{^{1}H} NMR (C_6D_6, 125 MHz):** δ 154.35 (*o*-Aryl*C*), 150.13 (*p*-Aryl*C*), 146.08 (Acridan*C*Se), ~128 (Acridan*C*), ~128 (Aryl*C*Se), ~128 (Acridan*C*), 124.79 (Acridan*C*H), 124.48 (Acridan*C*H), 123.14 (Acridan*C*Me), 122.70 (Acridan*C*N), 122.17 (Aryl*C*H), 71.80 (OCH$_2$), 58.66 (O*Me*), 37.36 (*C*Me$_2$), 34.75 (*p*-*C*HMe$_2$), 34.72 (*o*-*C*HMe$_2$), ~34.49 (C*Me$_2$*), 24.92 (*o*-CH*Me$_2$*), 24.25 (C*Me*). **^{77}Se{^{1}H} NMR (C_6D_6, 114 MHz):** δ 203.30 (s) **Anal. Calcd for $C_{55}H_{82}NSe_2O_4K$:** C, 64.87; H, 8.12; N, 1.38 %. **Found:** C, 64.56; H, 8.10; N, 1.41 %.

Potassium 4,5-bis(2,4,6-triisopropylphenyltellurido)-2,7,9,9-tetramethylacridanide · 2 dme {[K(ATe$_2^{Tripp2}$)(dme)$_2$]} (10): H[ATe$_2^{Tripp2}$] (50 mg, 0.056 mmol) and 1.2 eq. KCH$_2$Ph (8.7 mg, 0.056 mmol) were charged to a 25 ml round-bottom flask and then dissolved in ~10 ml of dme. The flask was appended to a vacuum line and immediately stirred, turning the solution from orange to bright yellow. The reaction was stirred at room temperature under argon for 15 minutes, after which the volatiles were removed *in vacuo*, and the residues dried for 20 minutes to afford a glassy yellow film. The flask was brought into the glovebox and 49.2 mg of yellow [K(ATe$_2^{Tripp2}$)(dme)$_2$] was collected (98 % yield). X-ray quality crystals were grown from dme/hexanes over 2 weeks at –30 °C. The solid can be stored for at least one year at –30 °C in an argon atmosphere. **^{1}H NMR (C_6D_6, 500 MHz):** δ 7.34 (s, 4H, ArC*H*), 7.03 (s, 2H, AcridanC*H*), 6.67 (s, 2H, AcridanC*H*), 4.19-4.11 (sept, $J_{H\text{-}H}$ 6.90 Hz, 4H, *o*-C*H*Me$_2$), 3.20 (s, 8H, OC*H$_2$*), 3.02 (s, 12H, O*Me*), 2.93-2.85 (sept, $J_{H\text{-}H}$ 7.20 Hz, 2H, *p*-C*H*Me$_2$), 2.07 (s, 6H, C*Me*), 1.70 (s, 6H, C*Me$_2$*), 1.37-1.36 (d, $J_{H\text{-}H}$ 6.89 Hz, 24H, *p*-CH*Me$_2$*), 1.29-1.28 (d, $J_{H\text{-}H}$ 6.89 Hz, 12H, *o*-CH*Me$_2$*). **^{13}C{^{1}H} NMR (C_6D_6, 125 MHz):** δ 156.17 (*o*-Aryl*C*), 150.26 (*p*-Aryl*C*), ~147 (Acridan*C*Me), 129.76 (Acridan*C*H), ~128 (Acridan*C*), 125.49 (Acridan*C*H), 125.19 (Acridan*C*Te), 122.62 (Aryl*C*Te), 121.52 (Aryl*C*H), 110.01 (Acridan*C*N), 71.96 (OCH$_2$), 58.63 (O*Me*), 40.05 (*o*-*C*HMe$_2$), 37.08 (*C*Me$_2$), 35.44 (C*Me$_2$*), 34.69 (*p*-*C*HMe$_2$), 25.36 (*o*-CH*Me$_2$*), 24.30 (*p*-CH*Me$_2$*), 21.09 (C*Me*). **^{125}Te{^{1}H} NMR (C_6D_6, 158 MHz):** δ 230.72 (s) **Anal. Calcd for $C_{55}H_{82}NTe_2O_4K$:** C, 59.22; H, 7.41; N, 1.26 %. **Found:** C, 59.97; H, 6.96; N, 1.62 %.

Reactions of 2,2,2-cryptand with 6, 9 or 10: In a glovebox, the appropriate potassium complex (**6**, 16.3 mg, 0.0213 mmol; **9**, 21.7 mg, 0.0213 mmol; **10**, 14.8 mg, 0.0133 mmol) was charged to a 20 ml scintillation vial with a stir bar and dissolved (or suspended) in ~0.5 ml of C_6D_6. Following this, 1 eq. of 2,2,2-cryptand (8.0 mg, 0.021 mmol {for **6** or **9**}; 5.0 mg, 0.013 mmol {for **10**}) was dissolved in ~2 ml of C_6D_6 and added dropwise to a stirring solution (or suspension) of **6**, **9** or **10** at room temperature. The reaction was stirred for 15 minutes, during which a bright yellow suspended precipitate was produced. The precipitate was allowed to settle and the supernatant was decanted and analyzed by NMR spectroscopy.

FOOTNOTES

† 16,540 of the 42,505 alkali metal-containing compounds in the CSD contain M–OR$_2$ (M = alkali metal) bonds. CSD accessed via Conquest (CSD version 5.43, updated November 2022).

‡ All metal–chalcogen distances in **3**-**6** and **9**-**10** are greater than the sum of the covalent radii (Li–S 2.33 Å, Li–Se 2.48 Å, K–S 3.08 Å, K–Se 3.23 Å, K–Te 3.41 Å),[42] but less than the sum of the Van der Walls radii (Li–S 4.0 Å, Li–Se 4.1 Å, K–S 4.6 Å, K–Se 4.7 Å, K–Te 4.9 Å).[81]

§ 98.9% of the K–OR$_2$ distances in the CSD fall within the range 2.60-3.20 Å. 100% of the non-bridging K–NAr$_2$ distances in the CSD fall within the range 2.61-2.89 Å. 100% of the bridging K–NAr$_2$ distances in the CSD fall within the range 2.758-3.105 Å. 100% of the bridging Li–N distances in the CSD fall within the range 1.89-2.253 Å. CSD accessed via Conquest (CSD version 5.44, updated June 2023).

¶ Geometry optimization of **9*** with only the K–Se distances constrained to crystallographic values resulted in a structure with a significantly overestimated K–N distance.

ASSOCIATED CONTENT

Supporting Information

The Supporting Information is available free of charge on the ACS Publications website.

NMR spectra, DFT data, SHAPE analysis (PDF).

DFT Structures (XYZ).

Accession Codes

CCDC 2286874−2286879 contain the supplementary crystallographic data for this paper. These data can be obtained free of charge via www.ccdc.cam.ac.uk/data_request/cif, or by emailing data_request@ccdc.cam.ac.uk, or by contacting The Cambridge Crystallographic Data Centre, 12 Union Road, Cambridge CB2 1EZ, UK; fax: +44 1223 336033.

AUTHOR INFORMATION

Corresponding Author

* David J. H. Emslie − *Department of Chemistry and Chemical Biology, McMaster University, Hamilton, Ontario, Canada, L8S 4M1; orcid.org/0000-0002-2570-9345*
Email: emslied@mcmaster.ca

Authors

Novan A. G. Gray − *Department of Chemistry and Chemical Biology, McMaster University, Hamilton, Ontario, Canada, L8S 4M1; orcid.org/0000-0003-3607-4063*

Ignacio Vargas-Baca − *Department of Chemistry and Chemical Biology, McMaster University, Hamilton, Ontario, Canada, L8S 4M1; orcid.org/0000-0002-3074-2051*

ACKNOWLEDGMENT

D.J.H.E. and I.V.B. thank NSERC of Canada for Discovery Grants. D.J.H.E. thanks the Digital Research Alliance of Canada (previously Compute Canada) for a 2020 Resources for Research Groups (RRG) grant. We are also grateful to Dr. James F. Britten in the McMaster X-ray diffraction facility and Dr. Jeffrey S. Price for helpful crystallographic discussions.

REFERENCES

1. (*a*) Pearson, R. G., Hard and Soft Acids and Bases. *J. Am. Chem. Soc.* **1963,** *85* (22), 35333-3539; (*b*) Pearson, R. G., Hard and soft acids and bases, HSAB, part I: Fundamental principles. *J. Chem. Educ.* **1968,** *45* (9), 581; (*c*) Pearson, R. G., Hard and soft acids and bases, HSAB, part II: Underlying theories. *J. Chem. Educ.* **1968,** *45* (10), 643; (*d*) Pearson, R. G., Acids and bases. *Science* **1966,** *151* (3707), 581; (*e*) Parr, R. G.; Pearson, R. G., Absolute hardness: companion parameter to absolute electronegativity. *J. Am. Chem. Soc.* **1983,** *105* (26), 7512-7516; (*f*) Ayers, P. W., An elementary derivation of the hard/soft-acid/base principle. *J. Chem. Phys.* **2005,** *122* (14), 141102; (*g*) Ho, T. L., The Hard Soft Acids Bases (HSAB) Principle and Organic Chemistry. *Chem. Rev*. **1975**, *75* (1), 1-20.

2. Olmstead, M. M.; Power, P. P., Structural characterization of a higher order cuprate: X-ray crystal structure of $[Li_3Cu_2Ph_5(SMe_2)_4]$. *J. Am. Chem. Soc.* **1989,** *111* (11), 4135-4136.

3. Olmstead, M. M.; Power, P. P., Isolation and first structural characterization of dimethyl sulfide solvates of phenyllithium, phenylcopper, and lower and higher order lithium phenylcuprate reagents. *J. Am. Chem. Soc.* **1990,** *112* (22), 8008-8014.

4. Olmstead, M. M.; Power, P. P., Synthesis and X-ray crystal structure of $[Li_2Cu_2(CH_2SiMe_3)_4(SMe_2)_2]_\infty$: the first detailed structural characterization of a lithium dialkylcuprate aggregate. *Organometallics* **1990,** *9* (6), 1720-1722.

5. M. Bolte, T. Kaese, M. Wagner, *CSD Communication*, 2023.

6. Champion, M. J. D.; Levason, W.; Pugh, D.; Reid, G., Neutral thioether and selenoether macrocyclic coordination to Group 1 cations (Li–Cs) – synthesis, spectroscopic and structural properties. *Dalton Trans.* **2015,** *44* (43), 18748-18759.

7. Jin, Y.; Kim, H. J.; Lee, J. Y.; Lee, S. Y.; Shim, W. J.; Hong, S. H.; Lee, S. S., Hard/Soft Heterometallic Network Complex of a Macrocycle with Endo/Exocyclic Coordination. *Inorg. Chem.* **2010,** *49* (22), 10241-10243.

8. Ryu, H.; Park, K.-M.; Ikeda, M.; Habata, Y.; Lee, S. S., A Ditopic O_4S_2 Macrocycle and Its Hard, Soft, and Hard/Soft Metal Complexes Exhibiting Endo-, Exo-, or Endo/Exocyclic Coordination: Synthesis, Crystal Structures, NMR Titration, and Physical Properties. *Inorg. Chem.* **2014,** *53* (8), 4029-4038.

9. Heller, M.; Sheldrick, W. S., Alkali Cation Ligating Chains and Sheets of the Macrocycle 1, 7-Dithia-18-Crown-6 with Bridging Iodo- and Thiocyanatocuprate(I) Units. *Z. fur Anorg. Allg. Chem.* **2003,** *629* (9), 1589-1595.

10. Röttgers, T.; Sheldrick, W. S., Lamellar Copper(I) Thiocyanate-Based Coordination Polymers containing the Alkali Cation ligating Thiacrown Ether 1,10-Dithia-18-crown-6. *Z. fur Anorg. Allg. Chem.* **2001,** *627* (8), 1976-1982.

11. Röttgers, T.; Sheldrick, W. S., Alkali Cation Ligating Iodocuprate(I)-Based Coordination Networks with the Thiacrown Ether 1,10-Dithia-18-crown-6. *J. Solid State Chem.* **2000,** *152* (1), 271-279.

12. Röttgers, T.; Sheldrick, W. S., One- to Three-Dimensional CuI and CuCN Based Coordination Polymers containing the Alkali Cation Ligating Thiacrown Ether 1, 10-Dithia-18-Crown-6. *Z. fur Anorg. Allg. Chem.* **2002,** *628* (6), 1305-1310.

13. Champion, M. J. D.; Dyke, J. M.; Levason, W.; Light, M. E.; Pugh, D.; Bhakhoa, H.; Rhyman, L.; Ramasami, P.; Reid, G., Sodium Thioether Macrocyclic Chemistry: Remarkable Homoleptic Octathia Coordination to Na^+. *Inorg. Chem.* **2015,** *54* (6), 2497-2499.

14. Kondo, Y.; Endo, K.; Hamada, F., Potassium–thiacalix[8]arene assembly: structure and guest sorption profiles. *Chem. Commun.* **2005,** (6), 711-712.

15. Kim, J.-Y.; Park, I.-H.; Lee, J. Y.; Lee, J.-H.; Park, K.-M.; Lee, S. S., Hard and Soft Metal Complexes of Calix[4]-bis-monothiacrown-5: X-ray and NMR Studies of Discrete Homodinuclear Complexes and a Heteromultinuclear Network. *Inorg. Chem.* **2013,** *52* (17), 10176-10182.

16. Santoro, O.; Elsegood, M. R. J.; Teat, S. J.; Yamato, T.; Redshaw, C., Lithium calix[4]arenes: structural studies and use in the ring opening polymerization of cyclic esters. *RSC Adv.* **2021,** *11* (19), 11304-11317.

17. Bilyk, A.; Hall, A. K.; Harrowfield, J. M.; Hosseini, M. W.; Skelton, B. W.; White, A. H., Systematic Structural Coordination Chemistry of *p-tert*-Butyltetrathiacalix[4]arene: 1. Group 1 Elements and Congeners. *Inorg. Chem.* **2001,** *40* (4), 672-686.

18. Yamada, M.; Kondo, Y.; Iki, N.; Kabuto, C.; Hamada, F., Hydrophobic and metal coordination interacted architecture based on *p-tert*-butylthiacalix[4]arene–potassium complex and its vapor absorption capability. *Tetrahedron Lett.* **2008,** *49* (24), 3906-3911.

19. Yamada, M.; Hamada, F., Thiacalix[4]arene–potassium assemblies: a supramolecular architecture based on coordination polymers and a dimeric structure based on triangular pyramidal arrangements. *CrystEngComm* **2011,** *13* (7), 2494-2499.

20. Huang, C.-A.; Ho, C.-L.; Chen, C.-T., Structural and catalytic studies of lithium complexes bearing pendant aminophenolate ligands. *Dalton Trans.* **2008,** (26), 3502-3510.

21. Mdluli, V.; Hubbard, P. J.; Javier-Jimenez, D. R.; Kuznicki, A.; Golen, J. A.; Rheingold, A. L.; Manke, D. R., A modular synthesis of tris(aryl)tren ligands: Synthesis, structure and lithiation chemistry. *Inorg. Chim. Acta* **2017,** *461*, 71-77.

22. Yin, Z.-B.; Wei, J.; Xi, Z., Trisyl-based multidentate ligands: synthesis and their transition-metal complexes. *Dalton Trans.* **2022,** *51* (9), 3431-3438.

23. Arnold, P. L.; Hall, J. J.; Natrajan, L. S.; Blake, A. J.; Wilson, C., Synthesis of mono- and di-potassium salts and methoxy adducts of sulfur-bridged biphenols by selective deprotonation. *Dalton Trans.* **2003,** (6), 1053-1055.

24. Farina, P.; Levason, W.; Reid, G., s-Block chalcogenoether chemistry – thio- and selenoether coordination with hard Group 2 ions. *Dalton Trans.* **2013,** *42* (1), 89-99.

25. Levason, W.; Pugh, D.; Purkis, J. M.; Reid, G., Complexes of Group 2 dications with soft thioether- and selenoether-containing macrocycles. *Dalton Trans.* **2016,** *45* (18), 7900-7911.

26. Cruz, C. A.; Emslie, D. J. H.; Harrington, L. E.; Britten, J. F., Single and Double Alkyl Abstraction from a Bis(anilido)xanthene Thorium(IV) Dibenzyl Complex: Isolation of an Organothorium Cation and a Thorium Dication. *Organometallics* **2008,** *27* (1), 15-17.

27. Vidjayacoumar, B.; Ilango, S.; Ray, M. J.; Chu, T.; Kolpin, K. B.; Andreychuk, N. R.; Cruz, C. A.; Emslie, D. J. H.; Jenkins, H. A.; Britten, J. F., Rigid NON- and NSN-ligand complexes of tetravalent and trivalent uranium: comparison of U–OAr_2 and U–SAr_2 bonding. *Dalton Trans.* **2012,** *41* (26), 8175-8189.

28. Andreychuk, N. R.; Ilango, S.; Vidjayacoumar, B.; Emslie, D. J. H.; Jenkins, H. A., Uranium(IV) Alkyl Complexes of a Rigid Dianionic NON-Donor Ligand: Synthesis and Quantitative Alkyl Exchange Reactions with Alkyllithium Reagents. *Organometallics* **2013,** *32* (5), 1466-1474.

29. Andreychuk, N. R.; Dickie, T.; Emslie, D. J. H.; Jenkins, H. A., Thorium(IV) alkyl and allyl complexes of a rigid NON-donor pincer ligand with flanking 1-adamantyl substituents. *Dalton Trans.* **2018,** *47* (14), 4866-4876.

30. Andreychuk, N. R.; Vidjayacoumar, B.; Price, J. S.; Kervazo, S.; Peeples, C. A.; Emslie, D. J. H.; Vallet, V.; Gomes, A. S. P.; Réal, F.; Schreckenbach, G.; Ayers, P. W.; Vargas-Baca, I.; Jenkins, H. A.; Britten, J. F., Uranium(IV) alkyl cations:

synthesis, structures, comparison with thorium(IV) analogues, and the influence of arene-coordination on thermal stability and ethylene polymerization activity. *Chem. Sci.* **2022,** *13* (46), 13748-13763.
31. Cruz, C.; Chu, T.; Emslie, D.; Jenkins, H.; Harrington, L.; Britten, J., Divergent reactivity of [(κ^3-L)ThCl$_2$(dme)] with Grignard reagents: Alkylation, ancillary ligand transfer to magnesium, and halide exchange caught in the act. *J. Organomet. Chem.* **2010,** *695*, 2798-2803.
32. Cruz, C. A.; Emslie, D. J. H.; Harrington, L. E.; Britten, J. F.; Robertson, C. M., Extremely Stable Thorium(IV) Dialkyl Complexes Supported by Rigid Tridentate 4,5-Bis(anilido)xanthene and 2,6-Bis(anilidomethyl)pyridine Ligands. *Organometallics* **2007,** *26* (3), 692-701.
33. Cruz, C. A.; Emslie, D. J. H.; Robertson, C. M.; Harrington, L. E.; Jenkins, H. A.; Britten, J. F., Cationic Thorium Alkyl Complexes of Rigid NON- and NNN-Donor Ligands: π-Arene Coordination as a Persistent Structural Motif. *Organometallics* **2009,** *28* (6), 1891-1899.
34. Vasanthakumar, A.; Gray, N. A. G.; Franko, C. J.; Murphy, M. C.; Emslie, D. J. H., Group 3 dialkyl complexes of a rigid monoanionic NNN-donor pincer ligand: synthesis, structures, unexpected reactivity with CPh_3^+, and hydroamination catalysis. *Dalton Trans.* **2023,** *52* (17), 5642-5651.
35. Motolko, K. S. A.; Emslie, D. J. H.; Jenkins, H. A., Yttrium and Aluminum Alkyl Complexes of a Rigid Bis-Anilido NON-Donor Ligand: Synthesis and Hydroamination Catalysis. *Organometallics* **2017,** *36* (8), 1601-1608.
36. Motolko, K. S. A.; Emslie, D. J. H.; Jenkins, H. A.; Britten, J. F., Potassium and Yttrium Complexes of a Rigid Bis-Phosphido POP-Donor Ligand. *Eur. J. Inorg. Chem.* **2017,** *2017* (22), 2920-2927.
37. Motolko, K. S. A.; Price, J. S.; Emslie, D. J. H.; Jenkins, H. A.; Britten, J. F., Zirconium Complexes of a Rigid, Dianionic Pincer Ligand: Alkyl Cations, Arene Coordination, and Ethylene Polymerization. *Organometallics* **2017,** *36* (16), 3084-3093.
38. Motolko, K. S. A.; Emslie, D. J. H.; Britten, J. F., Rigid NON-donor pincer ligand complexes of lutetium and lanthanum: synthesis and hydroamination catalysis. *RSC Adv.* **2017,** *7* (45), 27938-27945.
39. Wong, E. W. Y.; Emslie, D. J. H., Cyclometalation and coupling of a rigid 4,5-bis(imino)acridanide pincer ligand on yttrium. *Dalton Trans.* **2015,** *44* (25), 11601-11612.
40. Vasanthakumar, A.; Emslie, D. J. H.; Britten, J. F., Alkyl yttrium complexes of doubly cyclometallated xanthene- and naphthalene-backbone bis(phosphinimine) ligands. *J. Organomet. Chem.* **2019,** *903*, 120980.
41. Gray, N. A. G.; Price, J. S.; Emslie, D. J. H., Uranium(IV) Thio- and Selenoether Complexes: Syntheses, Structures, and Computational Investigation of U−ER$_2$ Interactions. *Chem. – Eur. J.* **2022,** *28* (1), e202103580.
42. Cordero, B.; Gómez, V.; Platero-Prats, A. E.; Revés, M.; Echeverría, J.; Cremades, E.; Barragán, F.; Alvarez, S., Covalent radii revisited. *Dalton Trans.* **2008,** (21), 2832-2838.
43. Klapötke, T. M.; Krumm, B.; Scherr, M., Studies on the Properties of Organoselenium(IV) Fluorides and Azides. *Inorg. Chem.* **2008,** *47* (11), 4712-4722.
44. Gronowitz, S.; Konar, A.; Hörnfeldt, A. B., ^{77}Se n.m.r. studies of organoselenium compounds: III—substituent effects in 4,4′-disubstituted diphenyl selenides and 4,4′-disubstituted diphenylmethanes studied by ^{1}H, ^{13}C and ^{77}Se spectroscopy. *Org. Magn. Reson.* **1977,** *9* (4), 213-217.
45. Prasad, C. D.; Balkrishna, S. J.; Kumar, A.; Bhakuni, B. S.; Shrimali, K.; Biswas, S.; Kumar, S., Transition-Metal-Free Synthesis of Unsymmetrical Diaryl Chalcogenides from Arenes and Diaryl Dichalcogenides. *J. Org. Chem.* **2013,** *78* (4), 1434-1443.
46. Champion, M. J. D.; Farina, P.; Levason, W.; Reid, G., Trivalent scandium, yttrium and lanthanide complexes with thia-oxa and selena-oxa macrocycles and crown ether coordination. *Dalton Trans.* **2013,** *42* (36), 13179-13189.
47. Hope, E. G.; Levason, W., Recent developments in the coordination chemistry of selenoether and telluroether ligands. *Coord. Chem. Rev.* **1993,** *122* (1), 109-170.
48. Hope, E. G.; Kemmitt, T.; Levason, W., Synthesis, properties, and multinuclear NMR (^{125}Te{^{1}H}, ^{13}C{^{1}H}, ^{1}H) studies in di- and polytelluroether ligands. *Organometallics* **1988,** *7* (1), 78-83.
49. Klapötke, T. M.; Krumm, B.; Mayer, P.; Polborn, K.; Schwab, I., Some Investigations on Organotellurium(IV) Cyanides. *Z. fur Anorg. Allg. Chem.* **2005,** *631* (13-14), 2677-2682.
50. Pérez-Balado, C.; Markó, I. E., 1-Iodo-1-selenoalkenes as versatile alkene 1,1-dianion equivalents. Novel connective approach towards the tetrahydropyran subunit of polycavernoside A. *Tetrahedron* **2006,** *62* (10), 2331-2349.
51. Bailey, P. J.; Coxall, R. A.; Dick, C. M.; Fabre, S.; Henderson, L. C.; Herber, C.; Liddle, S. T.; Loroño-González, D.; Parkin, A.; Parsons, S., The First Structural Characterisation of a Group 2 Metal Alkylperoxide Complex: Comments on the Cleavage of Dioxygen by Magnesium Alkyl Complexes. *Chem. – Eur. J.* **2003,** *9* (19), 4820-4828.
52. Harris, R. K.; Becker, E. D.; Cabral de Menezes, S. M.; Goodfellow, R.; Granger, P., NMR nomenclature. Nuclear spin properties and conventions for chemical shifts (IUPAC Recommendations 2001). **2001,** *73* (11), 1795-1818.
53. Dolomanov, O. V.; Bourhis, L. J.; Gildea, R. J.; Howard, J. K. A.; Puschmann, H., *OLEX2*: a complete structure solution, refinement and analysis program. *J. Appl. Crystallogr.*, **2009**, *42*, 339−341.
54. Sheldrick, G. M., Crystal Structure Refinement with SHELXL. *Acta Crystallogr., Sect. A: Found. Adv.*, **2015**, *71*, 3−8.
55. Sheldrick, G. M., Crystal Structure Refinement with SHELXL. *Acta Crystallogr., Sect. C: Struct. Chem.*, **2015**, *71*, 3−8.
56. Sluis, P. v. d.; Spek, A. L., BYPASS: An effective method for the refinement of crystal structures containing disordered solvent regions. *Acta Crystallographica Section A: Foundations of Crystallography* **1990,** *46* (3), 194-201.
57. (*a*) ADF 2020, SCM, Theoretical Chemistry, Vrije Universiteit, Amsterdam, The Netherlands, http://www.scm.com; (*b*) Guerra, C. F.; Snijders, J. G.; te Velde, G.; Baerends, E. J., Towards an order-N DFT method. *Theor. Chem. Acc.*, **1998**, *99* (6), 391-403; (*c*) te Velde, G.; Bickelhaupt, F. M.; Baerends, E. J.; Fonseca Guerra, C.; Van Gisbergen, S. J. A.; Snijders J. G.; Ziegler, T., Chemistry with ADF. *J. Comput. Chem.*, **2001**, *22* (9), 931-967
58. Perdew, J. P.; Burke, K.; Ernzerhof, M., Generalized Gradient Approximation Made Simple. *Phys. Rev. Lett.* **1996,** *77* (18), 3865-3868.
59. Lenthe, E. v.; Baerends, E. J.; Snijders, J. G., Relativistic regular two-component Hamiltonians. *J. Chem. Phys.* **1993,** *99* (6), 4597-4610.
60. van Lenthe, E.; Baerends, E. J.; Snijders, J. G., Relativistic total energy using regular approximations. *J. Chem. Phys.* **1994,** *101* (11), 9783-9792.
61. van Lenthe, E.; Ehlers, A.; Baerends, E.-J., Geometry optimizations in the zero order regular approximation for relativistic effects. *J. Chem. Phys.* **1999,** *110* (18), 8943-8953.
62. van Lenthe, E.; Snijders, J. G.; Baerends, E. J., The zero-order regular approximation for relativistic effects: The effect of spin–orbit coupling in closed shell molecules. *J. Chem. Phys.* **1996,** *105* (15), 6505-6516.
63. van Lenthe, E.; van Leeuwen, R.; Baerends, E. J.; Snijders, J. G., Relativistic regular two-component Hamiltonians. *Int. J. Quantum Chem.* **1996,** *57* (3), 281-293.
64. Grimme, S.; Antony, J.; Ehrlich, S.; Krieg, H., A consistent and accurate ab initio parametrization of density functional dispersion correction (DFT-D) for the 94 elements H-Pu. *J. Chem. Phys.* **2010,** *132* (15), 154104.
65. Grimme, S.; Ehrlich, S.; Goerigk, L., Effect of the damping function in dispersion corrected density functional theory. *J. Comput. Chem.* **2011,** *32* (7), 1456-1465.

66. Becke, A. D., A multicenter numerical integration scheme for polyatomic molecules. *J. Chem. Phys.* **1988,** *88* (4), 2547-2553.
67. Franchini, M.; Philipsen, P. H. T.; Visscher, L., The Becke Fuzzy Cells Integration Scheme in the Amsterdam Density Functional Program Suite. *J. Comput. Chem.* **2013,** *34* (21), 1819-1827.
68. Bérces, A.; Dickson, R. M.; Fan, L.; Jacobsen, H.; Swerhone, D.; Ziegler, T., An implementation of the coupled perturbed Kohn-Sham equations: perturbation due to nuclear displacements. *Comput. Phys. Commun.* **1997,** *100* (3), 247-262.
69. Jacobsen, H.; Bérces, A.; Swerhone, D. P.; Ziegler, T., Analytic second derivatives of molecular energies: a density functional implementation. *Comput. Phys. Commun.* **1997,** *100* (3), 263-276.
70. Wolff, S. K., Analytical second derivatives in the Amsterdam density functional package. *Int. J. Quantum Chem.* **2005,** *104* (5), 645-659.
71. R. F. W. Bader, *Atoms in Molecules: A Quantum Theory*, Clarendon Press, Oxford, 1990.
72. Rodríguez, J. I.; Bader, R. F. W.; Ayers, P. W.; Michel, C.; Götz, A. W.; Bo, C., A high performance grid-based algorithm for computing QTAIM properties. *Chem. Phys. Lett.* **2009,** *472* (1), 149-152.
73. Rodríguez, J. I.; Köster, A. M.; Ayers, P. W.; Santos-Valle, A.; Vela, A.; Merino, G., An efficient grid-based scheme to compute QTAIM atomic properties without explicit calculation of zero-flux surfaces. *J. Comput. Chem.* **2009,** *30* (7), 1082-1092.
74. Rodríguez, J. I., An efficient method for computing the QTAIM topology of a scalar field: The electron density case. *J. Comput. Chem.* **2013,** *34* (8), 681-686.
75. Ayers, P. W.; Jenkins, S., Bond metallicity measures. *Comput. Theor. Chem.* **2015,** *1053*, 112-122.
76. Tognetti, V.; Joubert, L., Density functional theory and Bader's atoms-in-molecules theory: towards a vivid dialogue. *Phys. Chem. Chem. Phys.* **2014,** *16* (28), 14539-14550.
77. Abramov, Y.A., On the Possibility of Kinetic Energy Density Evaluation from the Experimental Electron-Density Distribution. *Acta Crystallogr., Sect. A: Found. Crystallogr.*, **1997**, *A53*, 264-272.
78. Fradera, X.; Austen, M. A.; Bader, R. F. W., The Lewis Model and Beyond. *J. Phys. Chem. A* **1999,** *103* (2), 304-314.
79. Poater, J.; Solà, M.; Duran, M.; Fradera, X., The calculation of electron localization and delocalization indices at the Hartree–Fock, density functional and post-Hartree–Fock levels of theory. *Theor. Chem. Acc.* **2002,** *107* (6), 362-371.
80. NBO 6.0: E. D. Glendening, J. K. Badenhoop, A. E. Reed, J. E. Carpenter, J. A. Bohmann, C. M. Morales, C. R. Landis, and F. Weinhold, Theoretical Chemistry Institute, University of Wisconsin, Madison, 2013.
81. Batsanov, S. S., Van der Waals Radii of Elements. *Inorg. Mater.* **2001,** *37* (9), 871-885.

Table of Contents Graphic:

A family of rigid monoanionic pincer ligands featuring flanking neutral chalcogenoether (SR_2, SeR_2, TeR_2) donors and a central amido donor have been used to prepare a series of lithium and potassium complexes. The complexes were characterized crystallographically, spectroscopically, and computationally, and feature rare or unprecedented examples of M–ER_2 interactions (M = Li or K; E = S, Se, Te), allowing for a systematic investigation of hard alkali metal cation–soft chalcogenoether interactions.